Cancer Immunotherapy by Interleukin-21: Potential Treatment Strategies Evaluated in a Mathematical Model

Antonio Cappuccio, Moran Elishmereni, Zvia Agur

Institute for Medical Biomathematics (IMBM)
POB 282, Hate'ena St. 10, Bene-Ataroth 60991, Israel

Running title: Model for Cancer Immunotherapy by IL-21

Keywords: Melanoma/skin cancers; Sarcoma/soft-tissue malignancies; New algorithms; Cytokine gene therapy; Immunomodulation

Financial support: Marie Curie grant no.MRTN-CT-2004-503661 to A. C., and a grant from the Chai Foundation to Z. A. and M. E.

Requests for reprints: Moran Elishmereni, Institute for Medical Biomathematics (IMBM), PO Box 282, 10 HaTe'ena St., Bene-Ataroth 60991, Israel. Phone: 972-3-9733075; Fax: 972-3-9733410; E-mail: moran@imbm.org

Abstract

The newly-characterized Interleukin-21 (IL-21) plays a central role in the transition from innate immunity to adaptive immunity and shows substantial tumor regression in mice. IL-21 is now developed as a cancer immunotherapeutic drug, but conditions for efficacious therapy, and the cytokine's conflicting immunostimulatory and immunoinhibitory influence, are yet to be defined. We studied the effects of IL-21 on tumor eradication in a mathematical model focusing on NK-cell and $CD8^+$ T-cell-mediated lysis of tumor cells. Model parameters were estimated using results in tumor-bearing mice, treated with IL-21 via cytokine gene therapy (CGT), hydrodynamics-based gene delivery (HGD), or standard interval-dosing (SID). Our model accurately retrieved experimental growth dynamics in the non-immunogenic B16 melanoma and the highly-immunogenic MethA and MCA205 fibrosarcomas, showing a strong dependence of the NK-cell/$CD8^+$ T-cell balance on tumor immunogenicity. Moreover, in melanoma, simulations of CGT-like dosing regimens, dynamically-determined according to tumor mass changes, resulted in efficient disease elimination. In contrast, in fibrosarcoma, such a strategy was not superior to that of constant dosing protocols, HGD or SID. Our model supports clinical use of IL-21 as

a potent stimulator of cellular immunity against cancer, and suggests selecting the immunotherapy strategy according to tumor immunogenicity. Non-immunogenic tumors, but not highly-immunogenic tumors, should be controlled by IL-21 dosing, which depends on tumor mass at the time of administration. This method imitates, yet amplifies, the natural anticancer immune response, rather than accelerating only one of the response arms in an unbalanced manner.

Introduction

Despite the existence of numerous pathways in anticancer immunity, malignant cells effortlessly escape immune surveillance. The late and insufficient immune response to tumor challenge, as well as the wide array of immune evasion strategies employed by cancerous cells, enable an undisturbed disease progression (1). It seems, then, that artificial modulation of the natural immune response is necessary for an adequate immune attack against tumor cells. Specifically, rapid instigation of tumor-specific immunity and enhanced killing potential of immune effectors are essential for successful eradication of cancer (1).

The Interleukin-2 (IL-2) family of cytokines is well-known for its central involvement in the regulation of acquired immunity. A recently identified member of this family, which shares homology with IL-2, IL-4, and IL-15, is Interleukin-21 (IL-21), a product of activated $CD4^+$ T-helper cells (2). In both *in vitro* and *in vivo* studies, IL-21 directly modulates number and function of natural killer (NK) cells, dendritic cells (DCs), and lymphocytes (3, 4). Importantly, IL-21 enhances effector cell-mediated lysis of tumor cells, induces efficient antitumor immune memory, and significantly minimizes angiogenic and metastatic processes in numerous tumors (2, 5-10). The potent antitumor effect of IL-21 is attributed to its role in facilitating the transition from innate NK-cell responses to acquired cytotoxic $CD8^+$ T-cell responses. This is presumably achieved by inhibiting the former and stimulating the latter, and by enhancing the cytotoxic activity of both cell-types (2, 3, 11, 12).

The immunostimulatory effects of IL-21 motivated its development as an immunotherapeutic agent for the treatment of cancer. The increased safety of IL-21, as compared to IL-2, IL-15, and other immunotherapeutic factors (2, 5, 13, 14) further supports its clinical applicability. Yet, theoretically, the stimulatory effect of IL-21 on $CD8^+$ T-cells can be counter-balanced by its inhibitory influence on NK-cells and other factors of cell-mediated immunity (2, 11). These contradicting effects may limit the IL-21-induced antitumor response. Therefore, it seems mandatory to analyze the IL-21 net immunotherapeutic power in different oncological scenarios, prior to the establishment of an immunotherapeutic policy for this molecule.

Such analysis is enabled by biomathematically modeling IL-21 interactions with the involved immunologic and pathologic processes. Mathematical models have been previously employed for analyzing the effect of environmental disturbances on population survival, in general, and the effect of drug's inter-dosing intervals on chemotherapy efficacy/toxicity ratio, in particular (15). Analysis of individual tumor growth patterns in xenografted human ovary carcinoma spheroids was also possible by biomathematical modeling of complex angiogenesis-related processes (16). Another mathematical model describing detailed thrombopoiesis was employed for optimizing treatment strategies of thrombopoietin. The accuracy of the model's qualitative and quantitative predictions was prospectively validated in the preclinical setting (17). Recent mathematical models of tumor-immune interactions emphasize the relative role of certain effectors in anticancer responses, and evaluate efficacy of immunotherapy in the context of tumor challenge (18, 19).

In the current study, the antitumor effects of IL-21 under different oncological settings are evaluated in a mathematical model of the underlying biological processes. Following model's validation by published experimental data, we investigate IL-21 treatment strategies, and suggest efficacious protocols for eradicating or substantially attenuating tumor mass. A beneficial treatment should maximize IL-21-stimulated activation of adaptive immunity and, concurrently, minimize its negative effects on innate immunity. These conflicting aims for different tumor dynamics and immunogenicity levels will be investigated in this work.

Methods

The biological system at hand is first studied and its crucial interactions are pinpointed. This verbal model is then transformed into a mathematical model, which is implemented in the computer and simulated using experimentally evaluated biological parameters. Subsequently, we validate the model's prediction accuracy by using it to retrospectively retrieve independent experimental results. Following validation, the model is employed for simulating putative therapeutic scenarios and predicting their effects. These stages are elaborated below.

Biological Assumptions and Mathematical Model

As IL-21 has a central role in mediating the transition from initial NK-cell immunity to secondary T-cell immunity, this bipolar mechanism is highlighted in our model. Our assumption is that the direct effects of IL-21 on NK and $CD8^+$ T-cells are independent of other cell types, as shown in various murine experiments (4-10, 13, 14, 20-25). Relying on this recent

work, two classes of administration methods are examined here: drug application associated with tumor mass (Fig. 1A) and drug application being independent of tumor mass (Fig. 1B). The first method can be represented by cytokine gene therapy (hereafter CGT), in which genetically modified tumor cells continuously secrete IL-21 (5, 6). The second administration method can be represented by hydrodynamics-based gene delivery of DNA plasmids encoding large amounts of murine IL-21 (hereafter HGD), or standard interval-dosing (hereafter SID) of recombinant murine IL-21 (7, 13).

A concise mathematical description of the above scheme includes a system of ordinary differential equations (ODEs) describing six observables: [1] IL-21 concentration in the organism at any moment, [2] population dynamics of NK-cells in the spleen, [3] population dynamics of specific antitumor $CD8^+$ T-cells in the lymph nodes, [4] an element facilitating $CD8^+$ T-cell memory (see below), [5] a cytotoxic protein affecting tumor lysis, and [6] tumor mass at any moment. Effects of $CD4^+$ T-helpers, DCs and secondary chemokines are neglected, due to their minor role in the studied processes (5, 6, 9, 13). Reciprocal relations between $CD8^+$ T and NK-cells are not incorporated at this stage as well. Importantly, since the long-range consequences of IL-21 application are yet to be clarified, the evaluation of IL-21 effects on immune response is restricted here to a time-scale of weeks and to the primary tumor alone.

IL-21 dynamics. In our model the concentration of IL-21, denoted as u, is measured in units of ng/ml by the following equation

$$\dot{u} = input - \mu_1 u \tag{1}$$

with the initial condition $u_0 = u(t = 0)$. μ_1 serves as the clearance rate, and *input*, the function describing the route of drug administration, is mathematically detailed with respect to the two classes of administration methods (Fig. 1). In the first case (CGT), *input* is taken as proportional to the total number of genetically-engineered tumor cells, n:

$$input = hn.$$

This forms IL-21 dynamics as

$$\dot{u} = hn - \mu_1 u. \tag{2}$$

In contrast, in the latter case (HGD or SID), a pulse-like function centered at the application time is applied (see *parameter estimation* below).

NK-cell dynamics. The splenic NK population, x, is assumed to grow according to the logistic growth law, as defined by the equation

$$\dot{x} = r_1 x \left(1 - \frac{x}{h_1(u)}\right), \tag{3}$$

where r_1 is the growth rate, and the IL-21 effect on NK-cell population size is incorporated in $h_1(u)$, the carrying capacity in the logistic function. The latter component satisfies basic biological requirements: Firstly, the mean number of splenic NK-cells in normal conditions is considered constant, given by $x_0 = h_1(u = 0)$. This accounts for the high availability of NK-cells in stable health conditions (1, 26). Secondly, the effect of IL-21 on the growth of mouse NK-cells is apparently biphasic: at low drug doses NK proliferation is stimulated, while at higher doses it is inhibited (11, 27). However, as the positive effect on NK expansion is short-lived and observed mainly in the absence or low concentrations of other interleukins (11), and hence irrelevant to *in vivo* conditions, we address only IL-21's negative effect. Thus, the model considers IL-21-imposed reduction of NK-cells in a dose-dependent manner; $h_1(u)$ is selected as a monotonic decreasing function of IL-21. Thirdly, a saturation in the NK population is included, so it cannot decrease below the normal threshold x_{min}, the steady-state for NK dynamics for $u = \infty$. This limit is set within the normative biological range. The properties described are satisfied by the linear rational function

$$h_1(u) = \frac{p_1 u + p_2}{u + q_1}. \tag{4}$$

The above characteristics are translated into constraints for the parameters p_1, p_2, and q_1. In particular, the relations $x_0 = \frac{p_2}{q_1}$ and $p_1 = x_{min}$ can be derived. In allowing p_2 and q_1 to vary, while maintaining their ratio constantly equal to x_0, a one-parameter family of curves can be generated. A subsequent fit will enable to estimate the value of this parameter that interpolates the experimental behavior (see *parameter estimation* below).

CD8$^+$ T-cell dynamics. The IL-21-mediated expansion of naive and activated CD8$^+$ T-cells in both non-stimulated (4, 28-30) and stimulated conditions (5, 7, 13), suggests a robust influence of the cytokine on the carrying capacity of these cells. CD8$^+$ T-cells persist for many weeks post IL-21 application, allowing long-term protection against subsequent tumor inoculation (5, 7, 20, 22, 30). Distinct memory phenotypes observed in T-cell subsets following exposure to IL-21 (31) support this durable effect. Hence, we introduce an indirect factor m as an IL-21 dose-dependent product, that acts on CD8$^+$ T-cell expansion to enable an elongated adaptive response of these cells even after complete IL-21 clearance. Consequently, the dynamics of m are controlled by

$$\dot{m} = au - \mu_2 m, \tag{5}$$

where a represents the proportionality constant, and μ_2 is the clearance rate, the reciprocal of which is a measure of the duration of the CD8$^+$ T-cell response.

The tumor-specific CD8$^+$ T-subset in the lymph nodes, denoted by y, is

therefore described by the equation

$$\dot{y} = r_2 y \left(1 - \frac{y}{h_2(m)}\right) \tag{6}$$

with the initial condition $y_0 = h_2(m = 0)$, representing the number of such cells in a normal untreated setting. The logistic growth rate is r_2, and the carrying capacity h_2 is a function of the memory factor m, given by

$$h_2(m) = h_2(0) + \frac{\sigma m}{1 + \frac{m}{D}}. \tag{7}$$

The coefficient σ relates the growth of the carrying capacity to the memory factor (equation [5]). The actual limitation for specific $CD8^+$ T-cells, substantiated by recognized inhibitory functions of T-regulatory cells and Th2 cytokines (32), is enclosed in D. To maintain the system within realistic biological ranges, we assume that this expansion has an upper bound $y_\infty = h_2(0) + \sigma D$.

Cytotoxic-protein dynamics. Our model also accounts for the IL-21-mediated increase in effector-cell killing potential, by robust stimulation of cytolytic proteins, such as perforin and IFN-γ (2, 3, 10, 12, 33). This effect seems IL-21-dose-dependent in both $CD8^+$ T and NK-cells (5, 7, 13, 21, 28), and is described here by a cytotoxic protein, p. For simplicity, we assume production of this protein independently of the effector cells, thus negligible in IL-21-deprived conditions. These dynamics are given by

$$\dot{p} = \frac{b_1 u}{b_2 + u} - \mu_3 p, \tag{8}$$

where μ_3 denotes natural degradation of protein p within the standard biological ranges, and b_1 and b_2 are parameters of the chosen linear function. The initial condition is $p_0 = p(t = 0)$.

Tumor dynamics. Since the effect of IL-21 is not well-characterized in the context of subsequent cancer recurrence, we consider only primary tumor challenge (single inoculation). The total tumor cell number, n, evolves according to

$$\dot{n} = g(n) - k_1 p x n - k_2 p y n, \tag{9}$$

where $g(n)$ describes cancerous growth in non-treated mice. Tumors of different immunogenicities, a term used to define the capability of a cancer to naturally induce specific immune responses against itself, are included in the mathematical model: Specific non-immunogenic and highly-immunogenic tumor lines are investigated, thus $g(n)$ will be evaluated separately for each tumor, through fits of prior experiments in tumor-challenged control mice (see *parameter estimation* below). Tumor progression is affected by the cytotoxic (p-mediated) antitumor activity of $CD8^+$ T and NK-cells. Affinities

of tumor and NK or $CD8^+$ T-cell interactions are represented by k_1 and k_2, respectively.

As experimental measurements are restricted to tumor surface evaluation, equation [9] is modified to describe tumor size, measured in mm^2. A simple transformation between these properties requires a few basic assumptions. First, the initial condition $z_0 = z(t = 0)$ considers standard experimental methods: Tumor cells were inoculated in a solution, and developed a defined shape within a few days (5, 6, M. Ma- private communication). The corresponding simplified evaluation of tumor surface, is to divide the number of injected cells by the scale of a tumor cell surface, $10^{-6}mm^2$, so that, for instance, 10^5 cells will correspond to a size of 0.1 mm^2. Secondly, the tumor is thought to evolve as a homogenous sphere with a constant density volume. These considerations allow tumor volume, and tumor cell number (n), to be proportional to the amount $z^{3/2}$. Using the scale law $n \propto z^{3/2}$, and skipping the irrelevant coefficient, equation [9] is transformed into

$$\dot{z} = z^{-1/2} g(z^{3/2}) - k_1 pxz - k_2 pyz. \tag{10}$$

Collectively, the above equations constitute an autonomous ODE system. The positivity of the solutions, corresponding to positive initial conditions, is easily verified. Moreover, the immune system components x and y are always confined to the biological relevant strip $[x_{min}, x_0] \times [y_0, y_\infty]$.

Parameter Estimation

All simulations were performed using *matlab* programming. A fourth order Runge-Kutta integrator was applied to solve the ODEs, and the $curve - fitting\ toolbox$ was used for linear and exponential fits.

IL-21 dynamics. As tumor size is estimated through surface measurements, rather than through cell number, IL-21 dynamics (equation [2]) are formed as

$$\dot{u} = hz^{3/2} - \mu_1 u. \tag{11}$$

Since 10^5 genetically-modified tumorocytes were found to produce $\sim 2ng/ml$ of IL-21 in the course of one day (5), the constant h may be retrieved. Simply, if tumor size is considered to be unchanged within the first day, and the amount of IL-21 at the initial time is 0, IL-21 is estimated based on

$$\dot{u} \sim hz_0^{3/2} - \mu_1 u. \tag{12}$$

Equation [11], together with the conditions $u(0) = 0$ and $u(\bar{t} = 1\ \text{day}) = 2ng/ml$, gives

$$u(\bar{t}) = \frac{hz_0^{3/2}}{\mu_1}(1 - exp(-\mu_1 \bar{t})), \tag{13}$$

which implies that

$$h = \frac{\mu_1 u(\bar{t})}{z_0^{3/2}(1 - e^{-\mu_1 \bar{t}})}. \tag{14}$$

Given the values $z_0 \sim 10^{-1} mm^2$, $\mu_1 = 10\text{days}^{-1}$, $\bar{t} \sim 1$ day, h is estimated at $6.3 \cdot 10^2$ $mm^{-1}\cdot\text{days}^{-1}$.

As previously discussed, for HGD and SID the *input* function is formed as a pulse with an amplitude corresponding to the administered dose. For SID, the exponential decay rate was roughly estimated, since pharmacokinetic data of exogenous IL-21 is unavailable. The homology of IL-21 to IL-2 (4), whose decay rate was previously evaluated at $\mu_1 = 10$ days^{-1}, that is, a half-life in the range of a few hours (34), enabled to set the same value for IL-21. Conversely, IL-21 kinetics in HGD were achieved (Fig. 2A) by exponentially-fitting IL-21 concentrations monitored in this assay (13). Here, μ_1 was approximated at a much lower rate (0.5 days^{-1}), because of the continuous durable production of IL-21 in this method. In HGD simulations (described below), administration will be delayed by a day with respect to experiments, since plasma IL-21 levels were measured only 24 hours following injection.

NK-cell dynamics. Parameters for the logistic growth of NK-cells under no treatment were determined first. The carrying capacity was set here to the constant value $x_0 = 1.9 \cdot 10^6$ cells, an average of the NK populations counted in untreated mouse spleens (13). To estimate r_1, turnover rates of NK-cells were required, yet little is known regarding these rates in cancerous conditions. In normal states, mature mice or primates show a daily NK renewal rate of $\sim 2-5\%$ (26, 35), assumed to increase in presence of antigen. Hence, r_1 is set so that the rate of NK-cell replacement does not exceed a relative increment of 10% per day. Following strong reduction in the number of NK-cells, the dynamics can be well approximated by an exponential growth, and the ratio between population sizes of two consecutive days is simply e^{r_1}. A daily increment of 10% ($e^{r_1} = 1.1$) allows to calculate $r_1 = log(1.1)$. Near the carrying capacity, where the approximation of an exponential law is no longer valid and growth is slower, this percentage is generally decreased. For the parameter p_1, which denotes the lower threshold for NK numbers, a value within a biological range (10^4 cells) is designated.

Evaluation of the IL-21-mediated NK-cell decrease was based on an *in vivo* murine HGD study (13). Splenic NK-cells were counted one week after IL-21 administration, in a non-cancerous setting. IL-21 dynamics in HGD were applied in order to find the conditions under which the function $h_1(u)$ interpolates the two experimental points (Fig. 2B). The resulting values for p_2 and q_1 were $0.95 \cdot 10^6$ and $0.48 \cdot 10^6$ cells, respectively.

CD8$^+$ T-cells dynamics. The CD8$^+$ T-cells taken into account are tumor-antigen-specific populations. To determine parameters of IL-21-affected dynamics of CD8$^+$ T-cells, we used a study evaluating the response

to intraperitoneal injections of murine IL-21 in a thymoma line (7). Six $20\mu g$ doses (equivalent to $10\mu g/ml$ for a normal murine blood volume of 2 ml) administered on alternate days, with the decay rate $\mu_1 = 10$ days^{-1}, form IL-21 dynamics. CD8$^+$ T-cells were counted in draining lymph nodes (DLN) on days 5, 15, 30, and 45. To evaluate the initial number of specific CD8$^+$ T-cells,we assumed an exponential growth limited solely to the first two experimental points, as suggested by the global behavior. The resulting curve enabled to determine the exponential factor r_2 (at a value of 0.26 days^{-1}), and consequently lead to a rough approximation of the initial condition as 0.06% of DLN CD8$^+$ T-cells.

A maximum percentage of specific CD8$^+$ T-cell clones in the lymph nodes was set to be about 10% of those harvested in DLN ($y_\infty = \sigma D = 3{\cdot}10^6$ cells = 10% of $3 \cdot 10^7$ cells). The maximum was configured at $\sim 5-6\%$ of $3 \cdot 10^7$ cells at day 30 (P. Shrikant- private communication), allowing separate evaluation of D and σ. These latter two parameters are clearly dependent on the specific tumor model, as this ability is expected to be more pronounced in more immunogenic models. Since no experiments are available for evaluating the CD8$^+$ T-cell dynamics for a non-immunogenic model, values are roughly set at $\sigma = 2.1 \cdot 10^5$ cells·ml·days$^{-1} \cdot ng^{-1}$ and $D = 1.4 \cdot 10^{-3}$ days $\cdot ng \cdot ml^{-1}$. Finally, μ_2, the clearance parameter of m, is set to 0.01 days^{-1}, as the duration of the response was evaluated at ~ 100 days (5, 7), and parameter a is set as 0.01, in order to fit experimental data. These considerations form CD8$^+$ T-cell behavior (Fig. 2C).

Cytotoxic-protein dynamics. Lytic activity is elevated up to several weeks after primary challenge of genetically-modified tumor cells in CGT (5, 6) and normal tumor cells in HGD or SID (7, 13). Therefore, parameters were fixed so that μ_3^{-1} is in the range of tens of days. b_2, a measure of the concentration at saturation, is set at 0.1 $ng \cdot ml^{-1}$. This constant, along with b_1 (set within the range $10^{-2} - 10^{-1}$ days^{-1}), is evaluated by curve fitting.

Tumor dynamics. To describe the non-immunogenic B16 melanoma growth in control mice (5, 13), a logistic growth was assumed for the total number of tumor cells. Using the scaling law, this corresponds to the following equation for the tumor surface:

$$\dot{z} = r_3 z \left(1 - \frac{z^{3/2}}{K}\right), \tag{15}$$

which was fit with the observed data (Fig. 3A). For the immunogenic MethA fibrosarcoma (5), a linear growth for the tumor surface according to

$$\dot{z} = a \tag{16}$$

enabled an accurate fit of the dynamics in control mice (Fig. 3B). Of note, this implies that for such a model, tumor cell growth should obey a power law

function (36) with an exponent of $\frac{1}{3}$. The moderately-immunogenic MCA205 fibrosarcoma (13) was adequately described by an exponential growth (Fig. 3C).

Results

The mathematical model, containing the estimated biological parameters, was validated by examining its ability to retrieve experimental results of tumor growth in cancer-bearing mice, with or without IL-21 treatment (5, 13). Validation was extended to tumors of different immunogenicity, and to different administration routes, CGT and HGD. Following model validation, we examined different strategies of IL-21 therapy for cancers of varying immunogenicity and growth dynamics.

Model validation in CGT experiments. In the first experiment (5), inoculation of an immunogenic MethA IL-21-secreting fibrosarcoma ($2 \cdot 10^6$ cells at day 0) resulted in non-monotonic tumor growth (Fig. 4A, circles). These dynamics appeared comparable with tumor growth in untreated mice during the first week (Fig. 4A, squares), yet decreased thereafter towards complete elimination. Coinciding with the strong inhibition of NK-cells in highly-immunogenic tumors (1, 37), the immunogenic scenario (5) was reproduced in the model (Fig. 4A, bold line) with a low affinity value for the NK-tumor killing interaction. Simulations showed a primary rapid increase in tumor cells, due to lack of lysis in early stages of the response. The resulting high IL-21 concentrations lead to $CD8^+$ T-cell proliferation, and subsequent tumor eradication. The simulated behavior was generally in line with experimental curves, and with the observation that full immune control of the tumor was accomplished within approximately three weeks.

The second experiment, in which 10^5 cells of a non-immunogenic B16 IL-21-secreting melanoma were inoculated at day 0 (5), was also investigated by the mathematical model. In this scenario, complete elimination of the tumor was achieved in treated mice (Fig. 4B, circles), as compared to control mice (Fig. 4B, squares). Here, data from the previous study were not sufficient for characterizing the exact tumor dynamics. Still, experimental tumor development was minor and limited to the first 7 days after following treatment initiation (M. Ma- private communication). We simulated the model with a high NK-tumor affinity value, and achieved similar results of minimal or no tumor growth (Fig. 4B, bold line).

Experimental CGT results, leading to effective cancer regression, imply that the exact IL-21 concentrations in this method can be of therapeutic significance. To estimate this, we performed a model-independent analysis of the previously reported IL-21 production rates in CGT (5): In fibrosarcoma, the quantity $v = \int_0^t u(s)ds$ was calculated at $\sim 30\mu g \cdot ml^{-1} \cdot days$ for the first 20 days of therapy. This value implies that mean levels of circulating IL-21

during the antitumor activity are in the order of 1 $\mu g/ml$. In contrast, evaluation of mean IL-21 amounts in B16 melanoma was problematic, as tumor mass measurements were imprecise. Nevertheless, a value of ~ 10 ng/ml during the first therapeutic week is reasonable in this tumor-line. These dissimilarities suggest different requirements for IL-21-mediated elimination of tumors with varied immunogenicity.

To further elucidate these findings, we used our model to reproduce previous experiments of immunodeficient mice, challenged with IL-21-secreting B16-melanoma (5). Elimination of each effector type was accomplished by setting the corresponding tumor-affinity to 0. Model simulations (Fig. 4C-D, bold lines) were consistent with experimental curves (Fig. 4C-D, squares), where the IL-21-induced antitumor effect was significantly decreased in abrogation of NK or $CD8^+$ T-cells. However, different dynamics were observed for each case: Tumor growth under $CD8^+$ T-cell depletion was delayed at first, but accelerated later on, whereas in NK-depleted mice the opposite behavior was seen. Of note, retrieving experimental melanoma growth in normal IL-21-treated mice, as shown above (Fig. 4B), was not possible using tumor-effector affinity values derived from above simulations in depleted mice (data not shown). The fact that interactions between NK and $CD8^+$ T-cells and additional immune factors are not modeled, may lead to the inconsistency. This may also be attributed to well-known differences in the composition of the immune elements of depleted mice compared to normal mice (38).

Model validation in HGD experiments. We retrieved rejection of a non-immunogenic B16 melanoma and a moderately-immunogenic MCA205 fibrosarcoma, via intravenous gene delivery of IL-21 (13). In the experiment, two $20\mu g$ injections of mIL-21-expressing plasmids were administered in day 5 and 12 after tumor inoculation ($5 \cdot 10^5$ cells), and IL-21 concentrations followed previously-described kinetics (Fig. 2A). Our results show that the melanoma parameters, derived above for CGT, were sufficient for mimicking melanoma dynamics in HGD (Fig. 5A), and for leading to the appropriate change in NK-cell dynamics (Fig. 5B). Conversely, a satisfactory retrieval of fibrosarcoma growth (Fig. 5C) required different affinity values for tumor-effector interactions than those evaluated in CGT-fibrosarcoma simulations. This was in line with the different characterization of immunogenicity for this tumor type. The average concentration of circulating IL-21 produced by the administered plasmids during the first three weeks did not exceed 1 ng/ml, a lower value than in CGT. This result is corroborated by the limited tumor elimination shown in this HGD method, as compared to CGT (Fig. 4A-B). Overall, simulated growth fits experimental measurements in both tumor models described.

Model simulations of tumor-dependent IL-21 therapy. As the most effective tumor rejection was observed in tumor-dependent IL-21 therapy (Fig. 1A), such as CGT (5, 6, 20, 22), we used the model to simulate

this treatment in immunogenically-varying cancers. As CGT is clinically non-executable, a treatment strategy combining CGT and SID was simulated. The protocol consists of predetermined injection times, in conjunction with IL-21 doses that are dynamically adjusted during therapy, with respect to the tumor mass. In our simulations, IL-21 doses to be exogenously applied were set equivalent to the cytokine levels produced by the genetically-modified tumor of the corresponding size. Our model simulated this procedure for the non-immunogenic B16 melanoma and immunogenic MethA fibrosarcoma tumor lines, using their unique parameter sets, evaluated in the previous work stages.

In the simulated melanoma (10^5 tumor cells inoculated), the suggested protocol of 10 daily injections resulted in notable tumor rejection (Fig. 6A), dose intensities remaining in the range of ng/ml (Fig. 6B). The IL-21-mediated NK-cell inhibition was lower in the exogenous CGT-resembling therapy than in original CGT, coinciding with the lower total-IL-21 levels used in this interval-dosing protocol (data not shown). Notwithstanding, the simulated tumor remained controlled for several weeks, as in CGT (Fig. 4B). In contrast, simulating application of the same treatment protocol to immunogenic MethA fibrosarcoma ($2 \cdot 10^6$ tumor cells inoculated) resulted in incomplete tumor elimination (Fig. 6C), even though the administered IL-21 doses reached maximum values of 10 $\mu g/ml$ (Fig. 6D). These results indicate that both the immunogenic nature of the cancer and its size determine the success of tumor-dependent IL-21 therapy.

Discussion

In this work we have introduced a mathematical model for *in vivo* antitumor activity of IL-21 in mice. Our model, focusing on NK and T-cell immunity, was motivated by the irrefutable role of these cells in the IL-21-induced cancer control (2, 12). The model succeeded in retrieving the observed experimental behavior and strongly reflected well-established properties of cell-mediated antitumor immunity (1, 37). Thus, a high correlation between tumor immunogenicity and effector balance was shown in the simulations: Non-immunogenic melanoma tumors required high NK-cell lytic activity, as estimated in NK-tumor affinity values, whereas for the highly-immunogenic fibrosarcomas the opposite condition was necessary.

As in non-immunogenic tumors the activity of innate-phase effectors appears crucial, their destruction by the administered IL-21 must be prevented. In such cases, IL-21 levels that are relatively low (in the range of $\sim 10ng/ml$) seem most appropriate for small tumor mass, since IL-21 reduces the number of NK-cells in a dose-dependent manner. Indeed, full tumor elimination was achieved when simulating exogenous CGT-like therapy in non-immunogenic melanoma, that is, dynamic dosing of IL-21 according to tumor mass at the

time of administration.

IL-21 applied via CGT resulted in full tumor extinction in several experiments (5, 6, 20, 22), whereas HGD did not remove tumor completely (13). Our calculations show that mean IL-21 levels in CGT (10-10,000 ng/ml) are significantly higher than IL-21 concentrations in HGD (roughly 1 ng/ml). It can be argued, then, that dominating the success of CGT is the large IL-21 concentrations exerted in this method. However, this is not the case, since other administration strategies using similar, or even higher, IL-21 concentrations show ineffective tumor eradication (10, 23, 24). Rather, we hypothesize that CGT is successful due to the dependence of the administered IL-21 dose on tumor mass at any moment. In this way, a more natural stimulation of the immune response is achieved, avoiding abrogation of NK-cells when innate immunity is indispensable.

Though T-cell responses are dominant in tumor models of intensified immunogenicity, NK-cells may contribute via indirect mechanisms that aid T-cell function (1). Investigation of fibrosarcoma dynamics in NK-cell-depleted mice treated with IL-21 can further elucidate the nature of IL-21-stimulated immunity in immunogenic cancers. If NK-cells prove completely negligible in these circumstances, the use of high-dose ($\sim 10\mu g/ml$) IL-21 tumor-independent regimens, already from early disease stages, would appear a more reasonable treatment. Indeed, such drug concentrations were used in a recent murine study of IL-21 therapy in an immunogenic renal-cell carcinoma (25). Clinical implementation of such a strategy, however, should consider toxicity limitations, as in any intensified treatment. In another work (Cappuccio, Elishmereni, Agur, in preparation), we use the method of optimal control for fine-tuning the above-suggested tumor-dependent and independent immunotherapy regimens.

Incorporation of data regarding cytotoxic proteins (perforin, IFN-γ) elevated in various tumors responding to IL-21 administration (5, 6, 21, 33, 39), may provide insights on IL-21-mediated inflammation, allowing more detailed depiction of effector potential. Information of interleukins that cooperate with IL-21 to synergistically affect the immune response (8, 23, 40), may aid in evaluating mono-immunotherapy and potential combination immunotherapy. Humoral, anti-metastatic and anti-angiogenic properties of IL-21 (6, 8, 25) can interact with long-range effects of the drug on the immune response. Such effects should be investigated and implemented for extending the model beyond the scope of the current work.

IL-21 is continuously exhibiting therapeutic promise in its antitumor effects. The equivalence of IL-21 interactions in murine studies to the human system will determine the clinical implications of our findings. Validating the universality of our suggested model can pave the way for actual recommendations of IL-21 immunotherapy strategies, based on this work.

Acknowledgments

We thank Dr. Margery Ma, Dr. Vladimir Vainstein, Yuri Kogan, and Dr. Natalie Kalev-Kronik for valuable discussions and comments.

References

1. Janeway CA, Travers P, Walport M, Shlomchik M. Immunobiology. 6th ed. New York: Garland Science; 2005.

2. Sivakumar PV, Foster DC, Clegg CH. Interleukin-21 is a T-helper cytokine that regulates humoral immunity and cell-mediated anti-tumour responses. Immunology 2004;112(2):177-82.

3. Mehta DS, Wurster AL, Grusby MJ. Biology of IL-21 and the IL-21 receptor. Immunol Rev 2004;202:84-95.

4. Parrish-Novak J, Dillon SR, Nelson A, Hammond A, Sprecher C, Gross JA, et al. Interleukin 21 and its receptor are involved in NK cell expansion and regulation of lymphocyte function. Nature 2000;408(6808):57-63.

5. Ma HL, Whitters MJ, Konz RF, Senices M, Young DA, Grusby MJ, et al. IL-21 activates both innate and adaptive immunity to generate potent antitumor responses that require perforin but are independent of IFN-gamma. J Immunol 2003;171(2):608-15.

6. Di Carlo E, Comes A, Orengo AM, Rosso O, Meazza R, Musiani P, et al. IL-21 induces tumor rejection by specific CTL and IFN-gamma-dependent CXC chemokines in syngeneic mice. J Immunol 2004;172(3):1540-7.

7. Moroz A, Eppolito C, Li Q, Tao J, Clegg CH, Shrikant PA. IL-21 enhances and sustains CD8+ T-cell responses to achieve durable tumor immunity: comparative evaluation of IL-2, IL-15, and IL-21. J Immunol 2004;173(2):900-9.

8. Kishida T, Asada H, Itokawa Y, Cui FD, Shin-Ya M, Gojo S, et al. Interleukin (IL)-21 and IL-15 genetic transfer synergistically augments therapeutic antitumor immunity and promotes regression of metastatic lymphoma. Mol Ther 2003;8(4):552-8.

9. Nutt SL, Brady J, Hayakawa Y, Smyth MJ. Interleukin 21: a key player in lymphocyte maturation. Crit Rev Immunol 2004;24(4):239-50.

10. Takaki R, Hayakawa Y, Nelson A, Sivakumar PV, Hughes S, Smyth MJ, et al. IL-21 enhances tumor rejection through a NKG2D-dependent mechanism. J Immunol 2005;175(4):2167-73.

11. Parrish-Novak J, Foster DC, Holly RD, Clegg CH. Interleukin-21 and the IL-21 receptor: novel effectors of NK and T cell responses. J Leukoc Biol 2002;72(5):856-63.

12. Habib T, Nelson A, Kaushansky K. IL-21: a novel IL-2-family lymphokine that modulates B, T, and natural killer cell responses. J Allergy Clin Immunol 2003;112(6):1033-45.

13. Wang G, Tschoi M, Spolski R, Lou Y, Ozaki K, Feng C, et al. *In vivo* antitumor activity of interleukin 21 mediated by natural killer cells. Cancer Res 2003;63(24):9016-22.

14. Nakano H, Kishida T, Asada H, Shin-Ya M, Shinomiya T, Imanishi J, et al. Interleukin-21 triggers both cellular and humoral immune responses leading to therapeutic antitumor effects against head and neck squamous cell carcinoma. J Gene Med 2006;8(1):90-9.

15. Arakelyan L, Merbl Y, Agur Z. Vessel maturation effects on tumour growth: validation of a computer model in implanted human ovarian carcinoma spheroids. Eur J Cancer 2005;41(1):159-67.

16. Agur Z, Kheifetz Y. Resonance and anti-resonance: from mathematical theory to clinical cancer treatment design. Handbook of cancer models with applications to cancer screening, cancer treatment and risk assessment. In press 2005.

17. Skomorovski K, Harpak H, Ianovski A, Vardi M, Visser TP, Hartong SC, at al. New TPO treatment schedules of increased safety and efficacy: pre-clinical validation of a thrombopoiesis simulation model. Br J Haematol 2003;123(4):683-91.

18. De Pillis LG, Radunskaya AE, Wiseman CL. A validated mathematical model of cell-mediated immune response to tumor growth. Cancer Res 2005;65(17):7950-8.

19. De Pillis LG, Gu W, Radunskaya AE. Mixed immunotherapy and chemotherapy of tumors: modeling, applications and biological interpretations. J Theor Biol Epub 2005 Sep 6.

20. Ugai S, Shimozato O, Kawamura K, Wang YQ, Yamaguchi T, Saisho H, et al. Expression of the interleukin-21 gene in murine colon carcinoma cells generates systemic immunity in the inoculated hosts. Cancer Gene Ther 2003;10(3):187-92.

21. Brady J, Hayakawa Y, Smyth MJ, Nutt SL. IL-21 induces the functional maturation of murine NK cells. J Immunol 2004;172(4):2048-58.

22. Ugai S, Shimozato O, Yu L, Wang YQ, Kawamura K, Yamamoto H, et al. Transduction of the IL-21 and IL-23 genes in human pancreatic carcinoma cells produces natural killer cell-dependent and independent antitumor effects. Cancer Gene Ther 2003;10(10):771-8.

23. Zeng R, Spolski R, Finkelstein SE, Oh S, Kovanen PE, Hinrichs CS, et al. Synergy of IL-21 and IL-15 in regulating CD8+ T cell expansion and function. J Exp Med 2005;201(1):139-48.

24. Nelson A, Hughes S, Sivakumar P, Anderson M, Yen L, Shiota F, et al. Interleukin 21 enhances tumor specific immunity [abstract]. Proc Am Soc Clin Oncol 2003;22:171.

25. Hughes S, Chin L, Waggie K, Sivakumar P, Everson C, Clegg C. Interleukin 21 efficacy in a mouse model of metastatic renal cell carcinoma [abstract]. J Clin Oncol (Meeting Abstracts) 2004;22:2598.

26. Jamieson AM, Isnard P, Dorfman JR, Coles MC, Raulet DH. Turnover and proliferation of NK cells in steady state and lymphopenic conditions. J Immunol 2004;172(2):864-70.

27. Toomey JA, Gays F, Foster D, Brooks CG. Cytokine requirements for the growth and development of mouse NK cells *in vitro*. J Leukoc Biol 2003;74(2):233-42.

28. Kasaian MT, Whitters MJ, Carter LL, Lowe LD, Jussif JM, Deng B, et al. IL-21 limits NK cell responses and promotes antigen-specific T cell activation: a mediator of the transition from innate to adaptive immunity. Immunity 2002;16(4):559-69.

29. van Leeuwen EM, Gamadia LE, Baars PA, Remmerswaal EB, ten Berge IJ, van Lier RA. Proliferation requirements of cytomegalovirus-specific, effector-type human CD8+ T cells. J Immunol 2002;169(10):5838-43.

30. Li Y, Bleakley M, Yee C. IL-21 influences the frequency, phenotype, and affinity of the antigen-specific CD8 T cell response. J Immunol 2005;175(4):2261-9.

31. Eberl M, Engel R, Beck E, Jomaa H. Differentiation of human gamma-delta T cells towards distinct memory phenotypes. Cell Immunol 2002;218(1-2):1-6.

32. Seo N, Tokura Y. Downregulation of innate and acquired antitumor immunity by bystander gammadelta and alphabeta T lymphocytes with Th2 or Tr1 cytokine profiles. J Interferon Cytokine Res 1999;19(6):555-61.

33. Strengell M, Sareneva T, Foster D, Julkunen I, Matikainen S. IL-21 up-regulates the expression of genes associated with innate immunity and Th1 response. J Immunol 2002;169(7):3600-5.

34. Kirschner D, Panetta JC. Modeling immunotherapy of the tumor-immune interaction. J Math Biol 1998;37(3):235-52.

35. De Boer RJ, Mohri H, Ho DD, Perelson AS. Turnover rates of B cells, T cells, and NK cells in simian immunodeficiency virus-infected and uninfected rhesus macaques. J Immunol 2003;170(5):2479-87.

36. Hart D, Shochat E, Agur Z. The growth law of primary breast cancer as inferred from mammography screening trials data. Br J Cancer 1998;78(3):382-7.

37. Glas R, Franksson L, Une C, Eloranta ML, Ohlen C, Orn A, et al. Recruitment and activation of natural killer (NK) cells *in vivo* determined by the target cell phenotype. An adaptive component of NK cell-mediated responses. J Exp Med 2000;191(1):129-38.

38. Budzynski W, Radzikowski C. Cytotoxic cells in immunodeficient athymic mice. Immunopharmacol Immunotoxicol 1994;16(3):319-46.

39. Pelletier M, Bouchard A, Girard D. *In vivo* and *in vitro* roles of IL-21 in inflammation. J Immunol 2004;173(12):7521-30.

40. Strengell M, Matikainen S, Siren J, Lehtonen A, Foster D, Julkunen I, et al. IL-21 in synergy with IL-15 or IL-18 enhances IFN-gamma production in human NK and T cells. J Immunol 2003;170(11):5464-9.

Figure Legends and Figures

Fig. 1. Flow diagram of the modeled IL-21-induced antitumor mechanism. IL-21 accelerates the transition from innate NK-cell-mediated immunity to adaptive $CD8^+$ T-cell-mediated immunity, thereby eliciting an efficient immune response against target-cells. Administration of IL-21 is considered in two scenarios; dependent of tumor dynamics (A) or non-related to tumor dynamics (B). The recommended strategy of choice is assumed to take tumor immunogenicity into account.

Fig. 2. Fits of IL-21, NK-cell and $CD8^+$ T-cell dynamics based on

previous experiments (7, 13). (A) IL-21 dynamics following injection of 20 μg of HGD plasmids were reproduced according to experimental measurements (squares). (B) NK-cell dynamics in context of the above drug administration were simulated by interpolation of two experimental points at day 0 and 7 (indicated by squares) from the same study. (C) Standard drug-dosing of six IL-21 injections of $10\mu g/ml$ at days 2, 4, 6, 8, 10, and 12 produced $CD8^+$ T-cell dynamics, shown as an interpolation of four experimental points at days 5, 15, 30 and 45 (squares).

Fig. 3. Fits of tumor growth in control mice from previous studies (5, 13). The interpolating curves (bold lines) of B16 melanoma (A), MethA fibrosarcoma (B), and MCA205 fibrosarcoma (C) were selected as a modified logistic growth, linear growth, and exponential growth, respectively. Dynamics of all tumors are shown in reference to experimental behavior (thin lines).

Fig. 4. Simulations of fibrosarcoma and melanoma dynamics following IL-21 administration via CGT in normal and immunodeficient mice, with respect to a previous study (5). (A) Immunogenic MethA fibrosarcoma growth following experimental IL-21-CGT therapy in normal mice (thin line, circles) is reproduced by the model simulations (bold line). (B) Non-immunogenic B16 melanoma growth in similar conditions of drug application (circles) is simulated as well (bold line). Tumor growth in control mice is indicated in each case (thin line, squares). Experimental B16 melanoma growth in NK-cell-depleted (C) or T-cell-depleted (D) mice treated with IL-21 through CGT (thin line, squares) was similarly reproduced by model simulations (bold line).

Fig. 5. Simulations of melanoma and fibrosarcoma dynamics following IL-21 administration via HGD in mice, with respect to a previous study (13). (A) Application of 20 μg of IL-21-secreting plasmids at days 5 and 12 in mice inoculated with non-immunogenic B16 melanoma resulted in tumor dynamics (circles), which served for comparison with model simulations of tumor growth under an equal protocol (bold line), and to experimental tumor growth in control mice (thin line and squares). NK-cell dynamics under this treatment are presented as well (B). (C) MCA205 fibrosarcoma growth in mice treated with the same protocol (thin line and circles) is compared to the model simulations (bold line) and to experimental tumor growth in control mice (thin line and squares).

Fig. 6. Simulations of CGT-like IL-21 interval-dosing therapy in melanoma and fibrosarcoma. Murine B16 melanoma dynamics are predicted (A) in a CGT-based treatment protocol of 10 daily IL-21 intravenous injections (B). Murine MethA fibrosarcoma dynamics are predicted (C) under the same

treatment protocol (D). Horizontal lines in gray indicate threshold of initial tumor mass.

Figure 1:

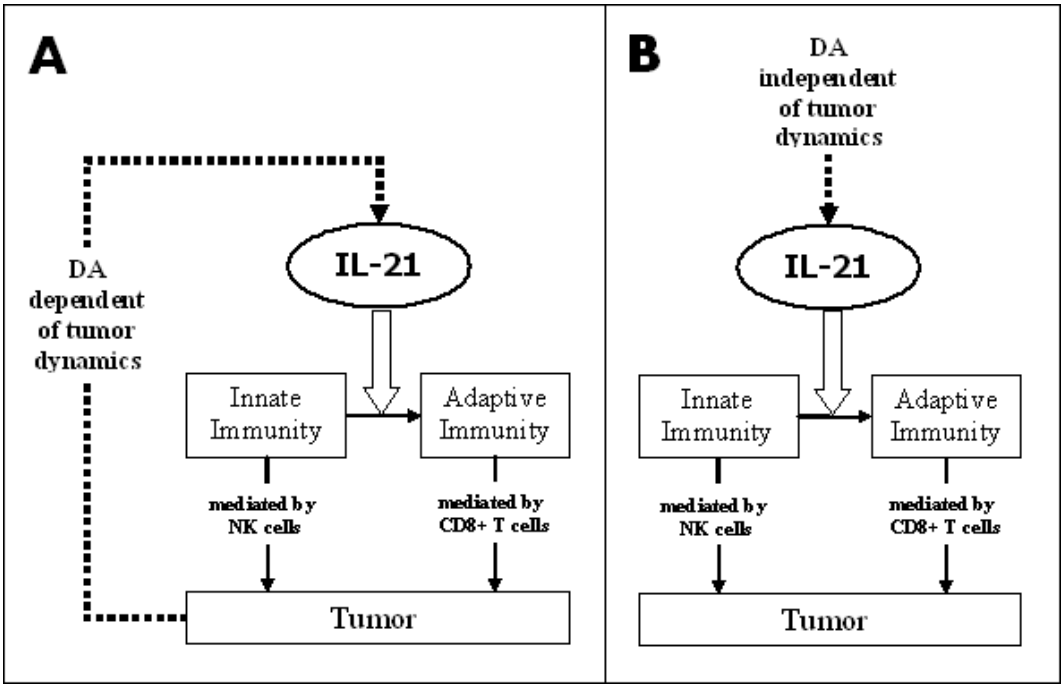
A
DA
dependent
of tumor
dynamics
IL-21
Innate
Immunity
Adaptive
Immunity
mediated by
NK cells
mediated by
CD8+ T cells
Tumor
B
DA
independent
of tumor
dynamics
IL-21
Innate
Immunity
Adaptive
Immunity
mediated by
NK cells
mediated by
CD8+ T cells
Tumor

Figure 2:

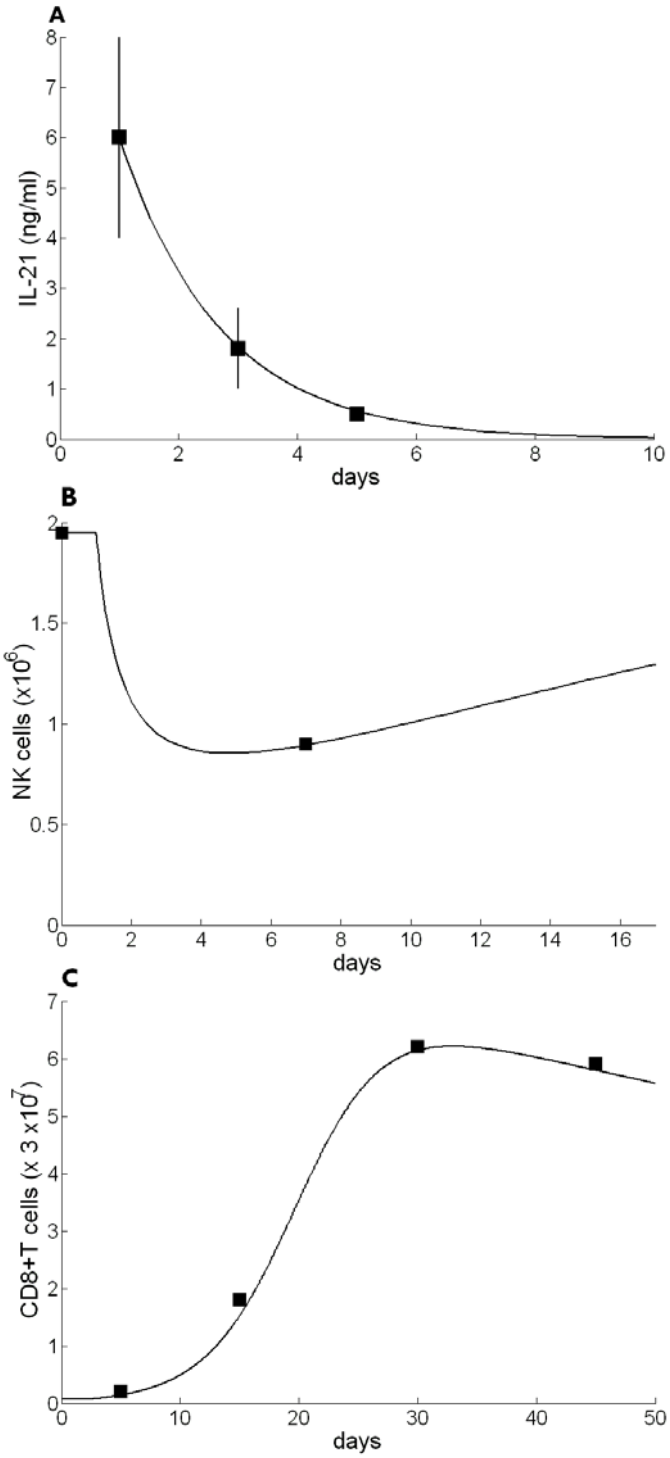

Figure 3:

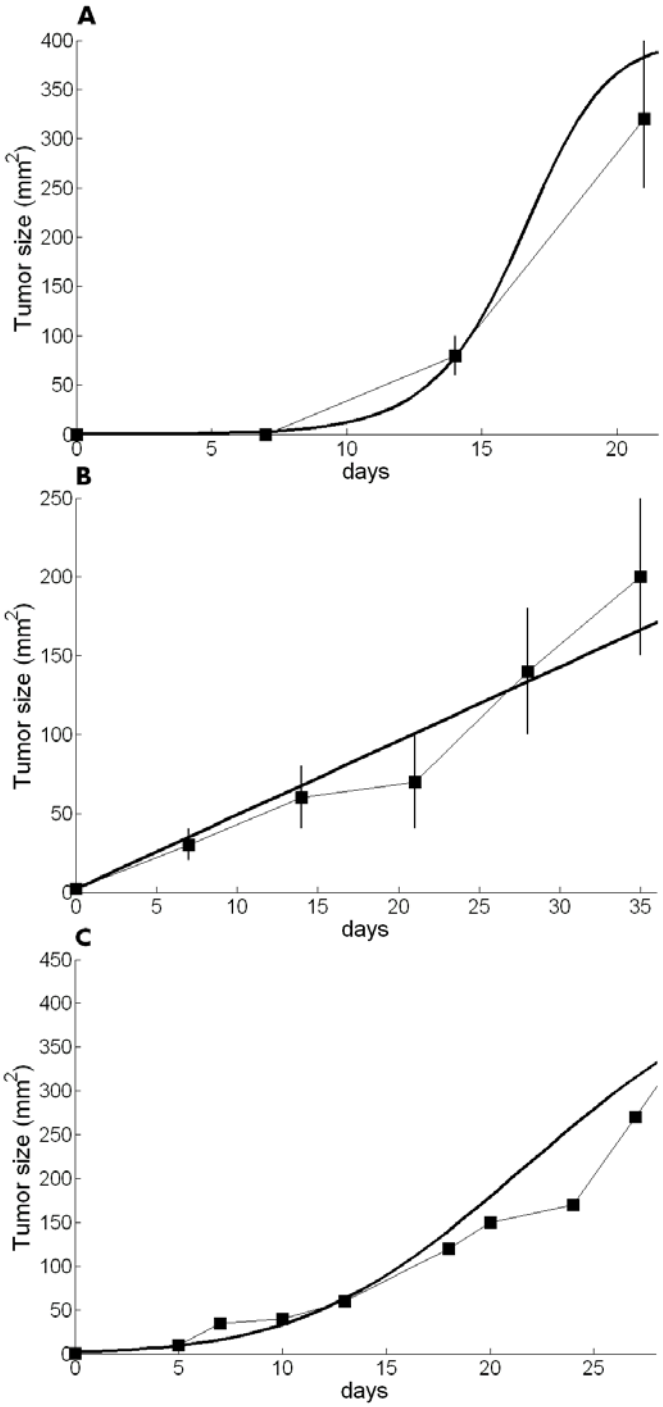
A
Tumor size (mm^2)
days
B
Tumor size (mm^2)
days
C
Tumor size (mm^2)
days

Figure 4:

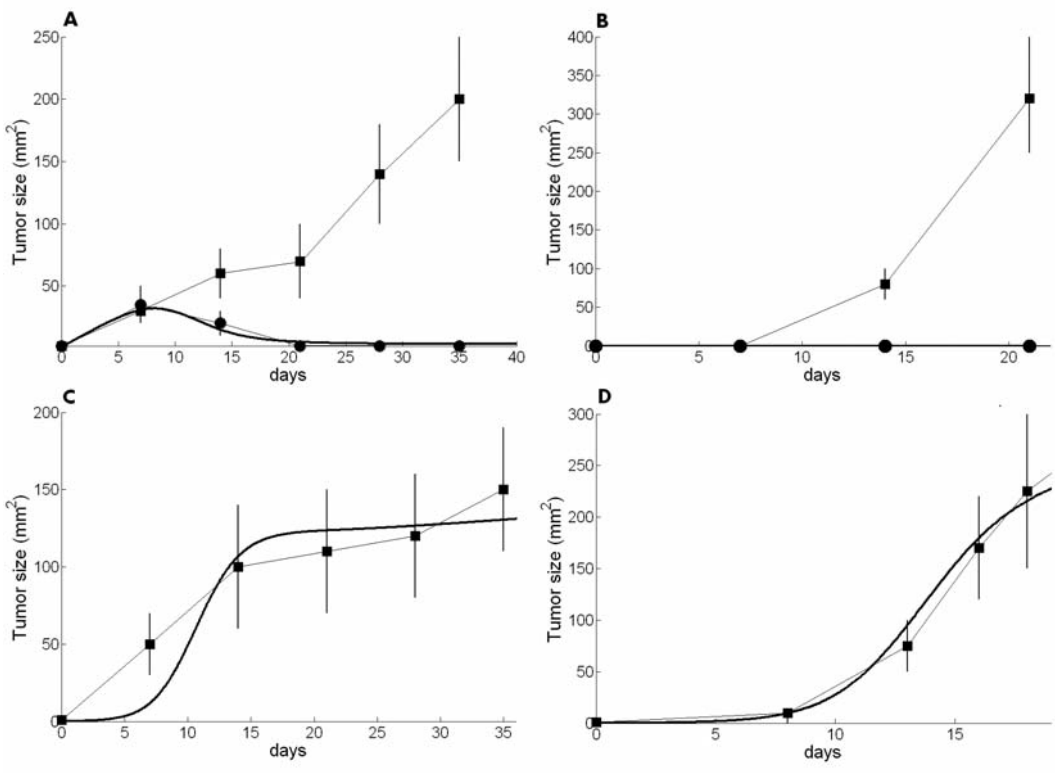

Figure 5:

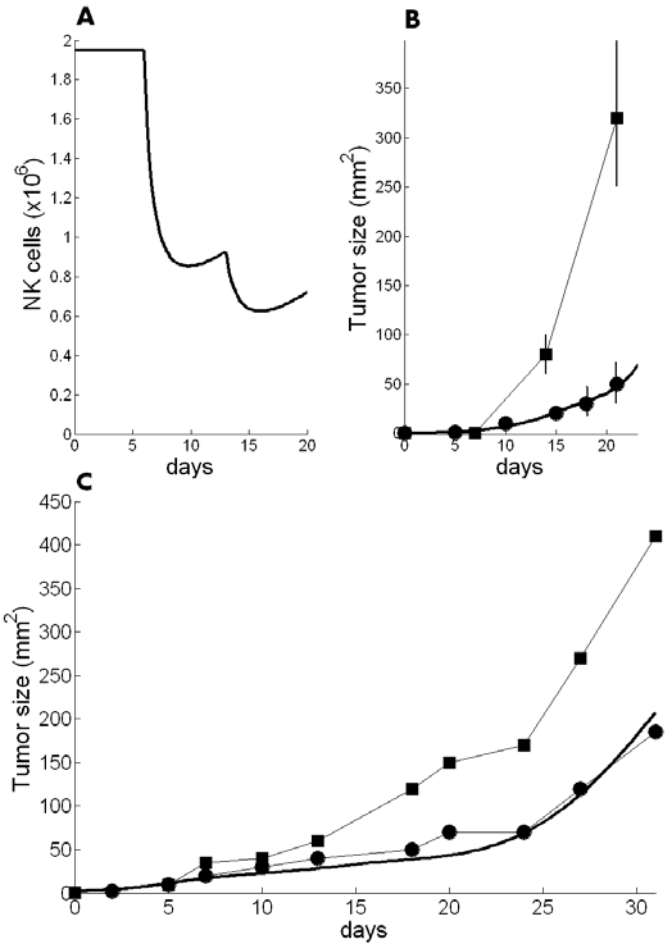
A
NK cells (x10^6)
days
B
Tumor size (mm^2)
days
C
Tumor size (mm^2)
days

Figure 6:

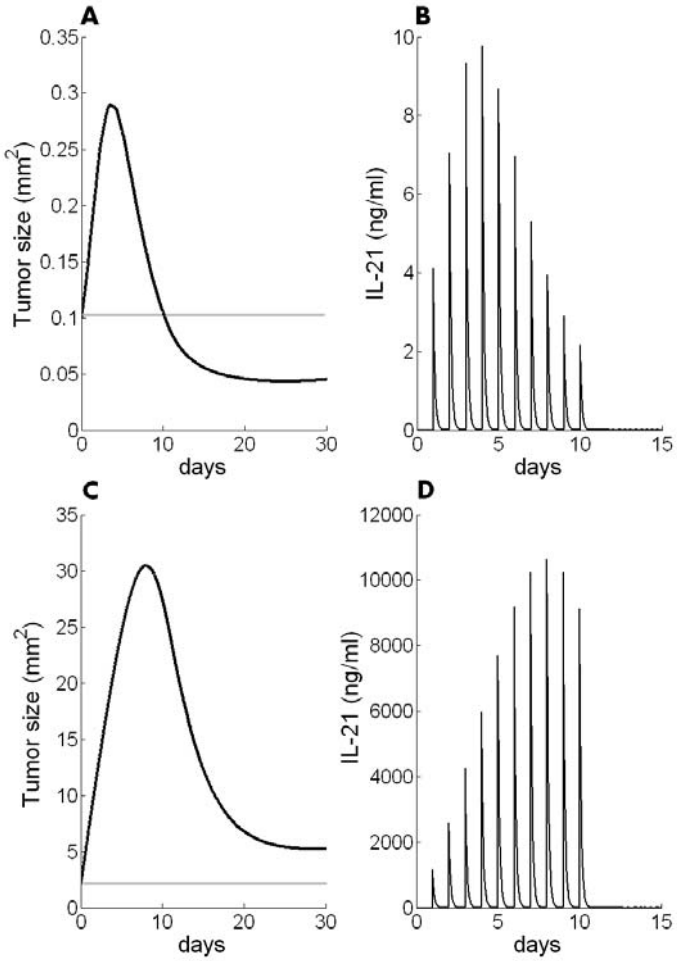
A
B
C
D
Tumor size (mm^2)
IL-21 (ng/ml)
days
0.35
0.3
0.25
0.2
0.15
0.1
0.05
0
10
8
6
4
2
30
20
5
15
12000
10000
8000
6000
4000
2000